Available online at www.sciencedirect.com

ScienceDirect

Energy Procedia 124 (2017) 31–37

Energy Procedia

www.elsevier.com/locate/procedia

7th International Conference on Silicon Photovoltaics, SiliconPV 2017

Optical and electrical characterization of poly-Si/SiO_x contacts and their implications on solar cell design

Frank Feldmann[a], Massimo Nicolai[b], Ralph Müller[a], Christian Reichel[a], Martin Hermle[a]

[a]*Fraunhofer Institute for Solar Energy Systems, Heidenhofstrasse 2, 79110 Freiburg, Germany*
[b]*ARCES, DEI – "Guglielmo Marconi", University of Bologna, Via Venezia 52, I-47521 Cesena (FC), Italy*

Abstract

The scope of this paper lies on the phenomenon of free-carrier absorption (FCA) in heavily phosphorus-doped poly-Si layers, applied at solar cells featuring poly-Si/SiO_x passivating contacts at the rear. Firstly, FCA is investigated on test structures featuring poly-Si contacts of different thickness and doping level. Secondly, these passivating contacts are integrated into the rear of solar cells featuring a boron-diffused emitter at the front. The infrared (IR) response of the solar cells is analyzed and FCA losses are quantified. In agreement with theory, it is shown that J_{sc} losses due to FCA increase with poly-Si doping level and thickness. For instance, a total J_{sc} loss of ~0.5 mA/cm² is obtained for a 145 nm thick poly-Si layer with a doping concentration of 1.9×10^{20} cm^{-3}.

© 2017 The Authors. Published by Elsevier Ltd.
Peer review by the scientific conference committee of SiliconPV 2017 under responsibility of PSE AG.

Keywords: free carrier absorption; passivating contacts; poly-Si; TOPCon

1. Introduction

Carrier-selective and passivating contacts can be ascribed a key role in improving the efficiency of crystalline silicon solar cells [1-5]. Recently, researchers at Kaneka achieved a new world-record of 26.6% efficiency by integrating the a-Si:H/c-Si heterojunction (HJT) into an IBC solar cell structure. Apart from that, passivating contacts which are based on an ultrathin SiO_x layer and a heavily-doped silicon film (e.g. poly-Si [6-9], SIPOS, or TOPCon [5]) have become an appealing alternative to heterojunction solar cells. This technology not only reduces minority carrier recombination to a level almost similar to HJT but also offers a higher tolerance to high-temperature processes, such as diffusion and firing [10, 11]. Hence, such passivating contacts hold the promise of a more cost-effective back-end process sequence.

1876-6102 © 2017 The Authors. Published by Elsevier Ltd.
Peer review by the scientific conference committee of SiliconPV 2017 under responsibility of PSE AG.
10.1016/j.egypro.2017.09.336

While there are plenty of papers dealing with the electrical properties of passivating contacts, such as surface passivation and contact resistivity, few papers deal with their optical properties. It has been shown that the absorption coefficient α of poly-Si resembles c-Si [12] and, thus, is lower than α of a-Si. Nevertheless, poly-Si contacts at the front side of a solar cell absorb about 0.5 mA/cm²/10 nm poly-Si [13]. By placing the passivating contact solely on the rear and using a homojunction at the front, parasitic absorption losses in the blue wavelength regime are avoided. Still the red response of the solar cell is affected by parasitic absorption losses, which separate into free carrier absorption (FCA) in poly-Si and absorption by the metal contact. On a lab scale, an efficiency of up to 25.7% has been achieved [14]. A first attempt to fabricate a comparable solar cell using industry-proven techniques resulted in an efficiency of 20.7% [10]. Among other losses, one significant loss was ascribed to FCA in the 200 nm thick, heavily P-doped poly-Si films at the rear.

Although, the absorption of infrared (IR) light due to FCA has been extensively studied for c-Si [15-17], the effect of poly-Si doping level and thickness has not been studied on solar cells yet. This paper addresses the optical and electrical characterization of n-type poly-Si/SiO_x contacts. Firstly, surface passivation of the poly-Si contacts is studied as a function of doping level and poly-Si thickness. Secondly, FCA coefficient is determined from spectrophotometer measurements. Finally, solar cells with poly-Si/SiO_x rear contact are shown and the impact of FCA is revealed.

2. Experimental details

2.1. Preparation and characterization of test structures

Symmetrical lifetime samples featuring different passivating contacts were realized on planar, (100) oriented n-type 1 Ωcm wafers. The following contact configurations were realized:

1) 35 nm poly-Si with $N_D = 5.5x10^{19}$ cm^{-3} ([P] = $1.5x10^{15}$ cm^{-2})
2) 90 nm poly-Si with $N_D = 1.19x10^{20}$ cm^{-3} ([P] = $3x10^{15}$ cm^{-2})
3) 145 nm poly-Si with $N_D = 1.29x10^{20}$ cm^{-3} ([P] = $4x10^{15}$ cm^{-2})
4) 145 nm poly-Si with $N_D = 1.67x10^{20}$ cm^{-3} ([P] = $5x10^{15}$ cm^{-2})
5) 145 nm poly-Si with $N_D = 1.90x10^{20}$ cm^{-3} ([P] = $6x10^{15}$ cm^{-2})

To this end, the wafers were cleaned according to the RCA procedure and a thin oxide layer was grown in boiling nitric acid. The poly-Si contacts were fabricated by low-pressure chemical vapor deposition (LPCVD) of intrinsic amorphous silicon and subsequently ion implantation of phosphorus (P) was performed. The ion dose and implantation energy were adjusted to the individual layer thicknesses. All wafers were then annealed at 850 °C for 30 min and finalized by a hydrogen passivation step at 425 °C for 25 min (RPHP [18]).

2.2. Preparation of solar cells and test structures

2x2 cm² solar cells were realized on n-type 1 Ωcm wafers with a thickness of 200 µm. The cells feature a homogeneous 150 Ω/sq boron emitter at the front which is well passivated by a stack of Al_2O_3 and SiN_x. At the rear passivating contacts as described in Sec. 2.1 were realized. Moreover, for the reference solar cells TOPCon featuring the same tunnel oxide layer but a PECVD SiC(n) layer was formed at the rear. Upon the high-temperature anneal the LPCVD a-Si films turned poly-crystalline while the a-SiC film remained amorphous as outlined in Ref. [19]. It should be noted that the poly-Si films had to be removed from the front by reactive ion etching as the LPCVD process always coats both sides of the wafer, in contrast to the PECVD TOPCon approach, which is strictly single sided.

The cells received an H-pattern grid on the front by means of thermal evaporation of Ti, Pd, and Ag and the lift-off technique. The contact fraction was about 1% and the shading due to the front metallization was ~1.1%. Thereafter, the solar cells were subjected to a hydrogenation process (RPHP) at 425 °C for 25 min. Finally, the rear side was metallized by thermal evaporation of Ag which makes a good contact and, more importantly, ensures a very high rear reflection.

2.3. Characterization

The surface passivation was measured on the symmetric lifetime samples using a Sinton WCT-120 lifetime tester [20]. The doping profiles were taken with the WEP CVP21 ECV profiler. It is commonly observed that the doping profile measured by ECV suggests a lower thickness than the real poly-Si thickness. This is likely due to the effect that some silicon ions react with the electrolyte and gaseous H_2 is released. Thereby, the etch current (etch rate) is underestimated but this effect can be accounted for by a valency correction (3.77 is commonly used for c-Si). In this experiment the depth of the doping profile of the poly-Si layer was expanded to the poly-Si thickness measured by spectroscopic ellipsometry. The used valency correction was in the range of 2.64-2.79.

For the determination of the free-carrier absorption, reflection and transmission was measured on the lifetime samples using a UV/Vis spectrophotometer. The measurement range was 1000 to 1500 nm with a step size of 2 nm. The FCA absorption was determined after the method described in Ref. [15].

The light *I-V* curves of the solar cells were taken in-house. Moreover, the *pFF* values were taken with a Sinton SunsVoc setup [21]. The quantum efficiencies and reflection of the solar cells was measured using the pv-tools LOANA setup. The step size was 10 nm.

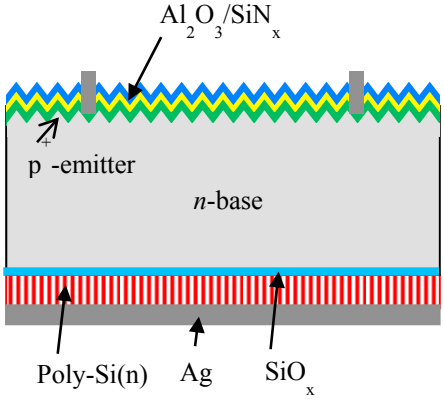

Fig 1. Schematic cross-section of the *n*-type Si solar cell with diffused front boron-doped emitter and full-area passivating rear contact (TOPCon or poly-Si).

3. Results

3.1. Surface passivation by poly-Si/SiO_x contacts

Fig. 2 plots the implied open-circuit voltages (iV_{oc}) and implied fill factor (*iFF*) values of the different poly-Si/SiO_x contacts measured after high-temperature anneal and hydrogen passivation process. The iV_{oc} values were in the range of 724-731 mV for all samples except for the 145 nm thick poly-Si contact featuring the highest doping level ([P] = $6x10^{15}$ cm^{-2}) . The latter showed a lower iV_{oc} value of about 715 mV. Moreover, the *iFF* values ranged from 85.1% to 86.6%. This underlines that all passivating contacts with the exception of the poly-Si/SiO_x contact having the highest doping level showed an excellent surface passivation at open-circuit and maximum power point conditions. In summary, a recombination prefactor J_0 as low as 2 fA/cm² was obtained by the 145 nm thick poly-Si contact having received a P dose of $4x10^{15}$ cm^{-2}. In turn, the highest J_0 value of 9 fA/cm² was obtained for the poly-Si contact with the highest doping level.

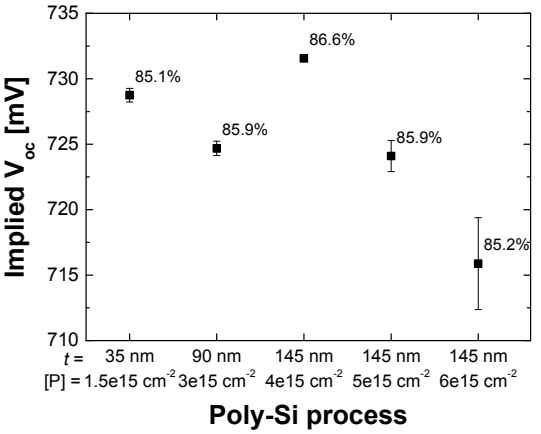

Fig. 2. Mean iV_{oc} and *iFF* of n-type poly-Si/SiO_x passivating contacts. The respective poly-Si thickness and P implantation dose are given.

3.2. Dopant profiles of poly-Si contacts and free carrier absorption

Fig. 3 shows the corrected doping profiles taken with an ECV profiler. In the poly-Si the dopants distributed quickly and a constant doping concentration was obtained. Following the flat profile, a steep drop occurred indicating the position of the interfacial oxide and the surface of the c-Si wafer. The doping tail within the c-Si was very shallow for all samples. The deepest profile of about 100 nm was found for the 145 nm poly-Si featuring the highest doping level. Thus, more than 95% of the dopants were confined to the poly-Si layer.

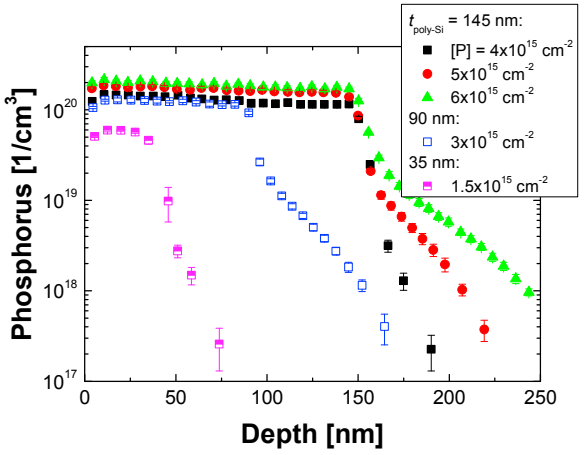

Fig. 3. Doping profiles obtained on poly-Si contacts after implantation of different P doses and high-temperature annealing.

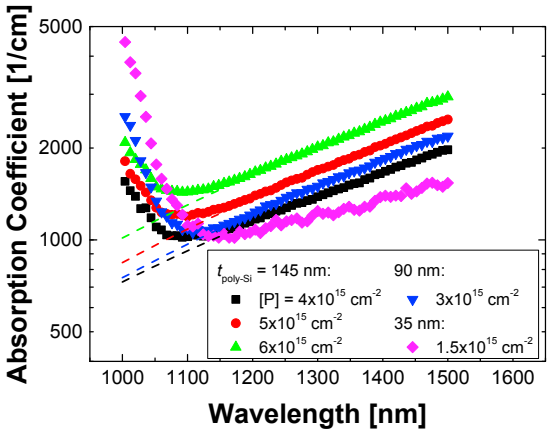

Fig. 4. Measured free carrier absorption coefficient for differently doped poly-Si(n) layers. The lines refer to the fits according to Eq. 1.

The free carrier absorption of the poly-Si contacts was determined after the method described in Ref. [15] using the R/T data taken by a UV/Vis spectrophotometer. Fig. 4 plots the absorption coefficient over wavelength for the different films. It is observed that FCA increased with doping level as suggested by theory. Moreover, the curves were fit to the equation:

$$\alpha_{FCA} = C * N_D * \lambda^x \quad (1)$$

in the wavelength range of 1200-1500 nm with N_D as variable input parameter. Since the signal of FCA was only moderate for the thinnest poly-Si film, thereby, introducing a large uncertainty, only the FCA curves of the 90 nm and 145 nm thick poly-Si films were fitted. As a result, a global optimum was found:

$$\alpha_{FCA} = 1.33 * 10^{-7} * N_D * \lambda^{2.58}, \quad (2)$$

which is in the range of the parameterization for c-Si [15].

3.3. Solar cells

Table I displays the solar cell results. The V_{oc} values were in the range of 679 to 691 mV. The J_{0e} of the passivated boron emitter was ~45 fA/cm² and, therefore, the V_{oc} was strongly limited by recombination at the front. Still the lowest V_{oc} of 679 mV was obtained for cells featuring the poly-Si/SiO_x contact with the highest doping level which exhibited a higher recombination current of ~9 fA/cm². On the other hand, the other passivating contacts showed comparably low J_0 values ≤ 5 fA/cm² and, thus, slightly higher V_{oc} values. The small fluctuations in V_{oc} from group to group are ascribed to a slightly fluctuating front side quality. Furthermore, each group showed mean *FF* values of about 81%. The mean *pFF* of all cells was in the range of 82.5% to 83.0%. By comparing SunsVoc and light *I-V* curve, the mean series resistance was determined to ~0.32 Ωcm². Thus, the different rear contacts showed a similar electrical behavior in terms of V_{oc} and *FF*. The highest J_{sc} values were measured for the TOPCon cells. The cells with poly-Si/SiO_x contacts having thicker layers exhibited 0.1-0.7 mA/cm² lower J_{sc} values. However, processing issues caused an inhomogeneous SiN_x deposition. Thus, the cells' reflection differed slightly. Hence, the parasitic absorption losses of the individual solar cell groups are analyzed by comparing the quantum efficiency measurements in the IR wavelength regime.

Table 1. Light *I-V* parameters obtained from 2x2 cm² solar cells. For each group the mean value of 14-21 cells is given.

Film thickness	Doping level (N_D = x10^{20} cm^{-3})	V_{oc} (mV)	J_{sc} (mA/cm²)	*FF* (%)	*pFF* (%)	Efficiency (%)
15 (TOPCon)	n/a	691.2±0.9	41.0±0.1	81.1±0.1	83.0±0.1	23.0±0.1
35	0.55	684.6±2.5	40.8±0.1	80.9±0.2	82.5±0.2	22.6±0.1
90	1.19	689.5±1.0	40.9±0.0	81.1±0.1	82.7±0.1	22.8±0.1
145	1.29	684.0±1.0	40.3±0.1	80.9±0.1	82.6±0.1	22.3±0.1
145	1.67	685.9±1.3	40.6±0.1	81.1±0.1	82.8±0.1	22.6±0.1
145	1.90	679.3±0.9	40.4±0.1	80.9±0.1	82.5±0.1	22.2±0.1

In order to quantify the parasitic absorption losses, external and internal quantum efficiency as well as reflectance are studied and compared to each other in the wavelength range of 900-1200 nm. For each group 7-14 solar cells were measured and analyzed. Fig. 5 plots a representative IQE (solid lines) and reflectance (dashed lines) curve of each solar cell group. Starting from 1000 nm, the IQE curves deviate from the IQE of the TOPCon reference cell. The thicker the poly-Si contact, the lower was the IQE at each given wavelength. As the passivation quality of all contacts is on the same high level, the reduced IQE in the IR regime indicates parasitic absorption losses in the poly-Si layers. Moreover, the reflection curves show a similar trend: the TOPCon reference had a reflection of 50% at 1200 nm, while the cell with 145 nm poly-Si contact had a reflection of <40% at 1200 nm.

Due to the very low minority carrier recombination at the rear, parasitic absorption at the rear is the only mechanism reducing the IQE. The parasitic absorption can be calculated as follows:

$$A_p = q \int_{900\,nm}^{1200\,nm} \phi_{AM1.5G}(\lambda) * (1 - R(\lambda) - EQE(\lambda)) d\lambda \quad (3)$$

The parasitic absorption in the IR is defined here as:

$$A_p = A_{FCA} + A_{metal}, \quad (4)$$

where A_{FCA} is the loss due to free carrier absorption and A_{metal} refers to parasitic absorption losses at the poly-Si/metal interface. With the assumption that FCA in the 15 nm thin, amorphous TOPCon contact is negligible, FCA in poly-Si can be easily calculated according to:

$$A_{FCA} = A_{p,TOPCon} - A_{p,poly-Si} \quad (5)$$

The total J_{sc} loss caused by the poly-Si contacts compared to the TOPCon cell is:

$$\Delta J_{sc} = q \int_{900\,nm}^{1200\,nm} \phi_{AM1.5G}(\lambda) * \left(EQE_{TOPCon}(\lambda) - EQE_{poly-Si}(\lambda)\right) d\lambda \quad (6)$$

Fig. 6 plots the calculated FCA losses (according to Eq. 3) and the total J_{sc} loss compared to the TOPCon cell where FCA losses are assumed to be zero. The FCA losses increased from 0.23 mA/cm² for 35 nm poly-Si through 0.52 mA/cm² for 90 nm poly-Si to 0.99 mA/cm² for 145 nm poly-Si. Likewise, the total J_{sc} loss increased up to 0.53 mA/cm² for 145 nm poly-Si (N_D = 1.90x10^{20} cm^{-3}). It can be seen that the total J_{sc} loss is smaller than the calculated FCA loss. As shown in Fig. 5 the reflection of the TOPCon cell was higher than the other cells, which means that a fraction of the additional photons which were not parasitically absorbed did not contribute to the cell's current but escaped at the front upon reflection at the rear. This effect is indicated by the red bars in Fig. 6.

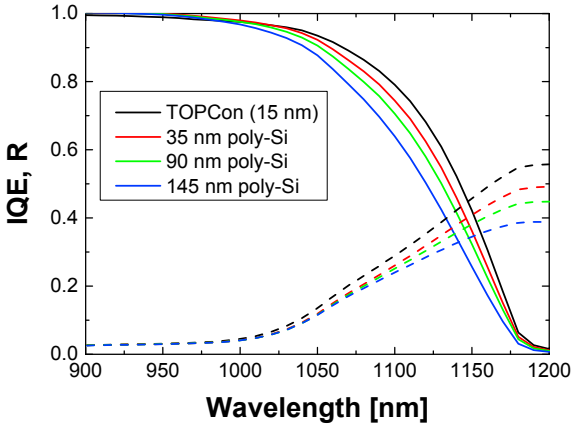

Fig. 5. Internal quantum efficiency (lines) and reflectance (dashed lines) curves of solar cells with different rear contact configurations.

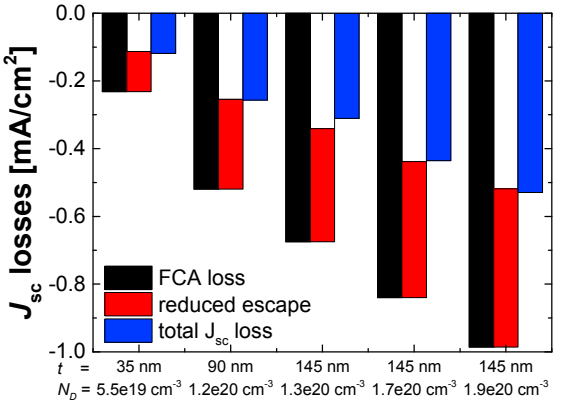

Fig. 6. Calculated FCA and total J_{sc} losses compared to reference cell featuring 15 nm TOPCon at rear.

4. Discussion

In summary, free carrier absorption in heavily phosphorus-doped poly-Si/SiO_x contacts has been studied by means of spectrophotometry on test structures as well as on solar cells. From the measured FCA curves, a parameterization for FCA in n-type poly-Si was extracted. Not surprisingly, it was in good agreement with the parameterization for c-Si. Finally, the effect of FCA has been studied on device level. A J_{sc} loss of about 0.53 mA/cm² due to FCA was obtained for a solar cell featuring a 145 nm thick poly-Si/SiO_x contact (N_D = 1.9x10^{20} cm^{-3}). Moreover, the general trend that FCA losses decrease with decreasing poly-Si thickness and poly-Si doping level was observed. Thus, in order to minimize FCA losses, the poly-Si thickness and doping level should be kept to a minimum. However, several authors have shown that the passivation quality of poly-Si/SiO_x contacts depends –amongst other things – on the doping level [7, 10, 13]. For instance, in Ref. [10] J_0 values < 5 fA/cm² were achieved with n-type poly-Si/SiO_x contacts featuring doping levels $N_D \geq$ 1x10^{20} cm^{-3}. Furthermore, such high doping levels promote low contact resistivities and, presumably, are necessary for screen-printed Ag contacts. Hence, the doping level of the poly-Si contact cannot be reduced well below N_D = 1x10^{20} cm^{-3} without sacrificing J_0 and/or υ_c. On the other hand, a reduced poly-Si thickness does not adversely affect the surface passivation provided that a minimum poly-Si thickness of about 15 nm is maintained [13]. Still it is questionable if such thin layers could be

contacted by screen-printing and firing as Ag pastes easily penetrate thin Si layers and would locally depassivate the passivating contact. Hence, for the design of poly-Si/SiO_x passivating rear contacts FCA losses and surface passivation as well as contact resistance have to be carefully balanced.

Acknowledgements

The authors would like to thank A. Leimenstoll, F. Schätzle, A. Seiler, S. Seitz, and A. Lösel for processing and E. Schäffer for measuring the solar cells. The authors also acknowledge M. Bauer who did the LPCVD poly-Si depositions at the RSC facility of the Department of Microsystems Engineering (IMTEK) of the Albert-Ludwigs-University in Freiburg. The work was funded by the Ministry of Economic Affairs and Energy under contract no. 0325877D “Upgrade-Si-PV”.

References

[1] D.D. Smith, P. Cousins, S. Westerberg, R. De Jesus-Tabajonda, G. Aniero, Y.C. Shen, Toward the Practical Limits of Silicon Solar Cells, Ieee J Photovolt, 4 (2014) 1465-1469.
[2] K. Masuko, M. Shigematsu, T. Hashiguchi, D. Fujishima, M. Kai, N. Yoshimura, T. Yamaguchi, Y. Ichihashi, T. Mishima, N. Matsubara, T. Yamanishi, T. Takahama, M. Taguchi, E. Maruyama, S. Okamoto, Achievement of More Than 25% Conversion Efficiency With Crystalline Silicon Heterojunction Solar Cell, Ieee J Photovolt, 4 (2014) 1433-1435.
[3] K. Yoshikawa, H. Kawasaki, W. Yoshida, T. Irie, K. Konishi, K. Nakano, T. Uto, D. Adachi, M. Kanematsu, H. Uzu, K. Yamamoto, Silicon heterojunction solar cell with interdigitated back contacts for a photoconversion efficiency over 26%, Nature Energy, 2 (2017) 17032.
[4] D. Adachi, J.L. Hernandez, K. Yamamoto, Impact of carrier recombination on fill factor for large area heterojunction crystalline silicon solar cell with 25.1% efficiency, Applied Physics Letters, 107 (2015).
[5] F. Feldmann, M. Bivour, C. Reichel, M. Hermle, S.W. Glunz, Passivated rear contacts for high-efficiency n-type Si solar cells providing high interface passivation quality and excellent transport characteristics, Solar Energy Materials and Solar Cells, 120 (2014) 270-274.
[6] U. Römer, R. Peibst, T. Ohrdes, B. Lim, J. Krügener, E. Bugiel, T. Wietler, R. Brendel, Recombination behavior and contact resistance of n+ and p+ poly-crystalline Si/mono-crystalline Si junctions, Solar Energy Materials and Solar Cells, 131 (2014) 85-91.
[7] U. Römer, R. Peibst, T. Ohrdes, B. Lim, J. Krugener, T. Wietler, R. Brendel, Ion Implantation for Poly-Si Passivated Back-Junction Back-Contacted Solar Cells, Ieee J Photovolt, 5 (2015) 507-514.
[8] D. Yan, A. Cuevas, J. Bullock, Y.M. Wan, C. Samundsett, Phosphorus-diffused polysilicon contacts for solar cells, Solar Energy Materials and Solar Cells, 142 (2015) 75-82.
[9] D. Yan, A. Cuevas, Y.M. Wan, J. Bullock, Passivating contacts for silicon solar cells based on boron-diffused recrystallized amorphous silicon and thin dielectric interlayers, Solar Energy Materials and Solar Cells, 152 (2016) 73-79.
[10] M.K. Stodolny, M. Lenes, Y. Wu, G.J.M. Janssen, I.G. Romijn, J.R.M. Luchies, L.J. Geerligs, n-Type polysilicon passivating contact for industrial bifacial n-type solar cells, Solar Energy Materials and Solar Cells, 158 (2016) 24-28.
[11] Y.G. Tao, V. Upadhyaya, C.W. Chen, A. Payne, E.L. Chang, A. Upadhyaya, A. Rohatgi, Large area tunnel oxide passivated rear contact n-type Si solar cells with 21.2% efficiency, Prog Photovoltaics, 24 (2016) 830-835.
[12] S. Reiter, N. Koper, R. Reineke-Koch, Y. Larionova, M. Turcu, J. Krügener, D. Tetzlaff, T. Wietler, U. Höhne, J.-D. Kähler, R. Brendel, R. Peibst, Parasitic Absorption in Polycrystalline Si-layers for Carrier-selective Front Junctions, Energy Procedia, 92 (2016) 199-204.
[13] F. Feldmann, C. Reichel, R. Muller, M. Hermle, The application of poly-Si/SiOx contacts as passivated top/rear contacts in Si solar, Solar Energy Materials and Solar Cells, 159 (2017) 265-271.
[14] A. Richter, J. Benick, F. Feldmann, A. Fell, M. Hermle, S.W. Glunz n-Type Si Solar Cells with Passivated Electron Contact: Identifying Sources for Efficiency Limitations by Wafer Thickness and Resistivity Variation Solar Energy Materials & Solar Cells, to be published (2017).
[15] S.C. Baker-Finch, K.R. McIntosh, D. Yan, K.C. Fong, T.C. Kho, Near-infrared free carrier absorption in heavily doped silicon, Journal of Applied Physics, 116 (2014).
[16] D.K. Schroder, R.N. Thomas, J.C. Swartz, Free Carrier Absorption in Silicon, IEEE Transactions on Electron Devices, 25 (1978) 254-261.
[17] C.M. Horwitz, R.M. Swanson, The Optical (Free-Carrier) Absorption of a Hole-Electron Plasma in Silicon, Solid State Electron, 23 (1980) 1191-1194.
[18] S. Lindekugel, H. Lautenschlager, T. Ruof, S. Reber, Plasma hydrogen passivation for crystalline silicon thin-films, in: Proceedings of the 23rd European Photovoltaic Solar Energy Conference, Valencia, Spain, 2008, pp. 2232-2235.
[19] F. Feldmann, M. Simon, M. Bivour, C. Reichel, M. Hermle, S.W. Glunz Efficient carrier-selective p- and n-contacts for Si solar cells, Solar Energy Materials & Solar Cells, (2014).
[20] R.A. Sinton, A. Cuevas, Contactless determination of current-voltage characteristics and minority-carrier lifetimes in semiconductors from quasi-steady-state photoconductance data, Applied Physics Letters, 69 (1996) 2510-2512.
[21] R.A. Sinton, A. Cuevas, A quasi-steady-state open-circuit voltage method for solar cell characterization, in: H. Scheer, B. McNelis, W. Palz, H.A. Ossenbrink, P. Helm (Eds.) Proceedings of the 16th European Photovoltaic Solar Energy Conference, James & James, London, UK, 2000, Glasgow, UK, 2000, pp. 1152-1155.